Theoretical Characterization of X-ray Absorption, Emission, and Photoelectron Spectra of Nitrogen Doped along Graphene Edges

ARTICLE *in* THE JOURNAL OF PHYSICAL CHEMISTRY A · DECEMBER 2012

Impact Factor: 2.69 · DOI: 10.1021/jp307405r · Source: PubMed

6 AUTHORS, INCLUDING:

Zhufeng Hou
Tokyo Institute of Technology
43 PUBLICATIONS **488** CITATIONS
SEE PROFILE

K. Terakura
National Institute of Advanced Industrial Scie…
374 PUBLICATIONS **13,151** CITATIONS
SEE PROFILE

THE JOURNAL OF PHYSICAL CHEMISTRY A

Article

pubs.acs.org/JPCA

Theoretical Characterization of X-ray Absorption, Emission, and Photoelectron Spectra of Nitrogen Doped along Graphene Edges

Xianlong Wang,*[,†,⊥] Zhufeng Hou,[†] Takashi Ikeda,[‡] Masaharu Oshima,[§] Masa-aki Kakimoto,[†] and Kiyoyuki Terakura[†,∥]

[†]Department of Organic and Polymeric Materials, Graduate School of Science and Engineering, Tokyo Institute of Technology, 2-12-1 S5-20 Ookayama, Tokyo 152-8552, Japan

[‡]Condensed Matter Science Division, Quantum Beam Science Directorate, Japan Atomic Energy Agency (JAEA), 1-1-1 Kouto, Sayo, Hyogo 679-5148, Japan

[§]Department of Applied Chemistry, The University of Tokyo, 7-3-1 Bunkyo-ku, Tokyo 113-8656, Japan

[∥]Research Center for Integrated Science, Japan Advanced Institute of Science and Technology (JAIST), 1-1 Asahidai, Nomi, Ishikawa 923-1292, Japan

ABSTRACT: K-edge X-ray absorption (XAS), emission (XES), and photoelectron (XPS) spectra of nitrogen doped along graphene edges are systematically investigated by using first-principles methods. In this study we considered pyridinium-like, pyridine-like, cyanide-like, and amine-like nitrogens at armchair and zigzag edges and pyrrole-like nitrogen at armchair edge as well as graphite-like nitrogen at graphene interior site. Our results indicate that nitrogen configuration and its location (armchair or zigzag edge) in nitrogen-doped graphene can be identified via the spectral analysis. Furthermore, some controversial spectral features observed in experiment for N-doped graphene-like materials are unambiguously assigned. The present analysis gives an explanation to the reason why the peak assignment is usually made differently between XPS and XAS.

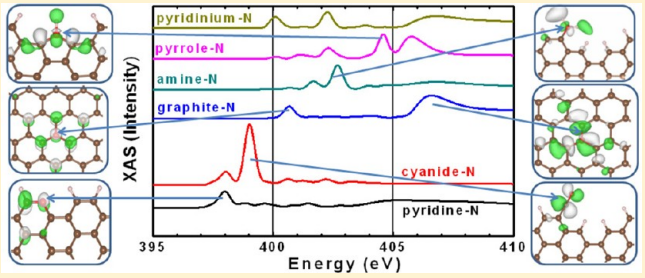

1. INTRODUCTION

Graphene has attracted extensive research interest since the first successful production, due to its excellent physical and chemical properties.[1] To realize wider applications of graphene, several physical or chemical features including interaction with substrates,[2−4] chemical doping, or adsorption[5−16] are adopted to modulate its mechanical and electronic properties. Among them, the doping of N or B having an electron more or less than C is an efficient method to modify the electronic properties, because they can be relatively easily substituted in graphene lattice due to their ionic radius close to that of C.

Although N-doped graphene (N-graphene) is conventionally synthesized from mixtures of carbon sources such as furan resin and N sources like phthalocyanine (Pc) by the carbonization at high temperature,[17] various chemical methods to synthesize N-graphene have been reported, including the reduction of graphene oxide in ammonia or nitrogen gas,[5] chemical vapor deposition,[6] nitrogen bombardment,[7] and nitrogen plasma treatment.[9] Both experimental and theoretical investigations suggest that N doping alters electronic properties of graphene significantly. Indeed, several groups reported that N-graphene-like materials exhibit surprisingly high oxygen reduction reaction (ORR) activity at the cathode of fuel cells.[17−31] Because both C and N are abundant elements on the earth, N-graphene is nowadays regarded as a promising material alternative to limited and expensive platinum, which is used as electrode catalysts in conventional fuel cells. Our previous theoretical studies show that the graphite-like N located at the zigzag edge of graphene can activate the neighboring edge-carbons toward ORR.[25−27] On the other hand, the most stable N configuration, namely, N at zigzag edges is suggested to reduce significantly the inherent ORR activity of graphene.[26] It is, therefore, necessary to first identify the N configurations in N-graphene for further enhancement of its catalytic performance.[29]

X-ray absorption (XAS), emission (XES), and photoelectron (XPS) spectroscopies are powerful techniques to gain the local electronic and structural information of materials under study. In fact, most of N configurations in N-graphene are successfully identified by using these techniques;[8,9,30−43] however, the assignment of some spectral features actually observed is still under debate. For example, among the four observed peaks of the N K-edge XAS, the second lowest excitation-energy peak was assigned to cyanide-like N (i.e., −CN) by Niwa et al.[30] whereas it was attributed to amine-like N (i.e., $-NH_2$) by Zhang et al.[35] and Zhong et al.[41] Furthermore, the N 1s XPS

Received: July 26, 2012
Revised: December 25, 2012
Published: December 27, 2012

peak at around 399.9−400.2 eV was assigned to cyanide-like N by Ray et al.,[39] whereas Pels et al.[40] ascribed it to pyrrole-like N. Somewhat more puzzling is the fact that three main contributions from the lower binding energy (or excitation energy) are usually assigned differently between XPS and XAS even if both spectra are measured and analyzed by the same group.[30,31]

To understand these spectral features for N-graphene more clearly, theoretical efforts have also been turned to this subject.[44] Nonetheless, the N 1s XPS was theoretically investigated by employing graphene flakes, in which edge structures are not well-defined. Furthermore, to the best of our knowledge, systematic theoretical simulations for XAS, XES, and XPS of N doped at graphene edges have not been performed yet. Recall that both types of graphene edges influence various macroscopic properties of synthesized N-graphene. For example, some moieties of pyridine-like N coordinating Fe ion at armchair edges, which can open an electronic band gap of graphene,[45] are considered as an active site for ORR.[22] On the other hand, zigzag edges of graphene, where edge states are localized,[46] can exhibit attractive properties such as ORR activity[25] and electronic spin transport,[47,48] provided that nitrogens are doped at the above-mentioned proper positions or the edges are appropriately terminated. Therefore, systematic investigations of XAS, XES, and XPS for N located along either armchair or zigzag edges are required to identify the N configurations more precisely. For this purpose, in this paper, the computed spectra of N doped at armchair and zigzag edges in graphene are presented and the possible configurations of N along the edges are discussed in detail. Our analysis makes significant contributions to solving the controversial aspects described above and also explains the reason why the assignment of peaks is made differently between XPS and XAS.

The remainder of this paper is organized as follows. Section 2 describes the computational methods for electronic structures and X-ray spectra. Section 3 presents the results for the subjects described in the preceding paragraph. Finally, we draw conclusions in Section 4.

2. COMPUTATIONAL DETAILS

The spectral calculations were performed by using the 6-311G** basis sets for fully relaxed atomic positions in the Gaussian augmented plane wave all-electron formalism[49] as implemented in CP2K code.[50] The cutoff of charge density for solving the Poisson equation was set to 280 Ry. Only Γ point was sampled. The relative stability among some configurations of two doped N atoms along the armchair edge was studied by employing a plane-wave basis set and ultrasoft-pseudopotentials, as implemented in the PWSCF package in Quantum Espresso suite.[51] The generalized gradient approximation of Perdew−Burke−Ernzerhof[52] was used for exchange and correlation functionals of the density functional theory. Energy cutoffs for wave function and charge density were set to 35 and 350 Ry, respectively. The Brillouin zone was sampled using 4 × 1 × 1 Monkhorst-Pack mesh for the supercells described below.

The supercells of graphene nanoribbons in the present calculations are shown in Figure 1. The armchair (zigzag) nanoribbon contains 12 (6) zigzag chains and 5 (10) armchair rows as displayed in Figure 1a (1b). For the zigzag edge we include dihydrogenation, which is suggested in previous works to play a crucial role in controlling the distribution of N along the zigzag edge.[29,55] The respective size of supercell along

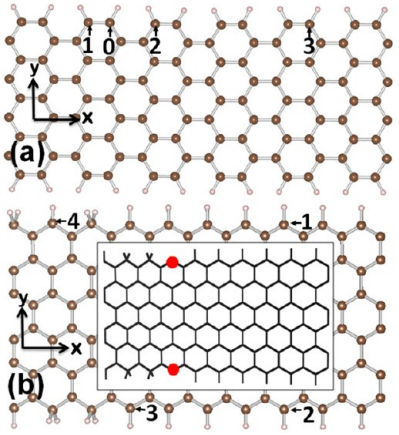

Figure 1. Models of graphene nanoribbons with armchair (a) and zigzag (b) edges are schematically shown. The numbered sites are candidates for N dopants. In the actual calculations, a model for a given N configuration has one type of N dopant along each edge and is symmetric with respect to a mirror plane perpendicular to the *y* axis. An example is shown in the inset of (b) for $C_{H2}z_{pyd}C_H$. C, H, and N are represented by large dark brown and small thin brown and large red balls, respectively.

aperiodic *y*- and *z*-directions was chosen as 30 and 20 Å to avoid the interaction with periodic images.

For these supercells, we checked the convergence of the above-mentioned computational conditions. First, we adopted larger cutoff energies (40 Ry for wave function and 400 Ry for charge density) and used 6 × 1 × 1 Monkhorst−Pack mesh. The largest change in the relative energies listed in Table 1 is only 1 meV. Second, to check the reliability of the Γ point calculation adopted by CP2K, we repeated the calculations for the above relative energies using PWSCF with Γ point sampling and the original smaller cutoff energies. The largest change in the relative energies in Table 1 is 0.02 eV. This accuracy is high enough for the spectral analysis.

Table 1. Total Energies (eV) for Two Pyridinium-Like or Pyridine-Like N Dopants at Armchair Edge in Far, Middle, and near Configurations Shown in Figure 1 [a]

dopant type	far	middle	near
pyridinium-like	0.000	0.313	0.910
pyridine-like	0.000	0.146	0.441

[a]The total energy of the far configuration is set to zero for each dopant type.

We make two additional remarks about the structures of doped N configurations. First, for amine-like N, we consider the configurations shown schematically around NH_2 in Figure 2. In contrast to other cases, the amine-like moiety may take parallel configurations (Figure 2a,c) in which H−H of $-NH_2$ is parallel to the graphene plane or perpendicular configurations (Figure 2b,d) in which the same H−H is perpendicular to the graphene plane for each of armchair and zigzag edges. Second, the use of nanoribbons will impose some constraint to possible atomic configurations. We consider that the pyrrole case may be an example of such a case. Therefore, the study of pyrrole case will be supplemented by cluster calculations where we use the structures shown in Figure 3. Detailed discussion on relative stability among different configurations and spectral features for these structures will be given in the following sections.

dx.doi.org/10.1021/jp307405r | J. Phys. Chem. A 2013, 117, 579−589

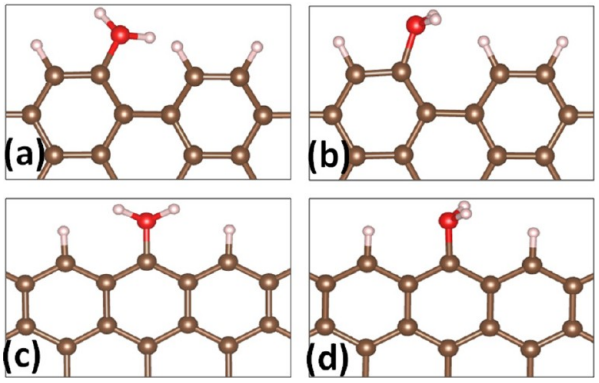

Figure 2. Models of amine-like N: (a) and (b) armchair edge; (c) and (d) zigzag edge. Only local structures are shown. In the parallel configurations ((a) and (c)), H−H of amine-like N is parallel to the graphene plane, whereas in the perpendicular ones ((b) and (d)), H−H is perpendicular to graphene plane.

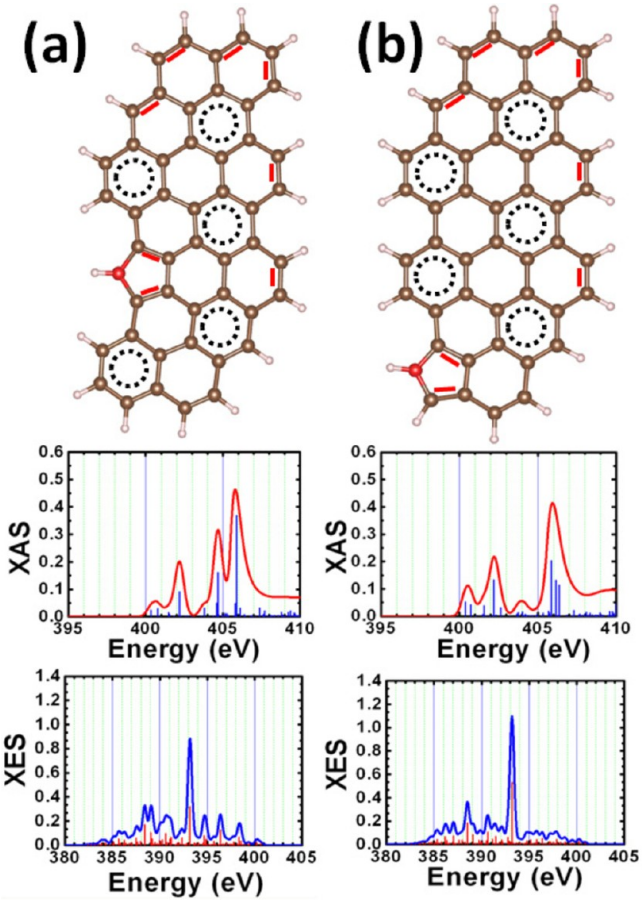

Figure 3. Two pyrrole-like N configurations in a cluster model. The circles and red bars denote Clar sextets and double bonds. The XAS and XES spectra for each configuration are shown in the lower panels.

The method for the calculation of spectral features is basically the same as in our previous paper[29] except the calculation of core-level binding energy. Namely, XAS and XES spectra were obtained in Slater's transition potential framework[53] as described in ref 28. On the other hand, the N 1s core-level binding energy E_b(N 1s) with respect of the Fermi level was evaluated by the following three approaches: (1) Kohn−Sham orbital energy; (2) total energy difference (ΔSCF); 3) Slater's transition state. In the second approach, the actual quantity that we calculated in the present work is slightly different from that in the previous paper[29] and is given by

$$E_b(\mathrm{N1s};\Delta\mathrm{SCF}) = E_{tot}(n_c-1,n_v) - E_{tot}(n_c,n_v-1) \quad (1)$$

where the first term in the right-hand side is the total energy of a system with one core hole, the second term is that with one electron removed from the Fermi level.[54] This expression is simple and easy to calculate. Moreover, it shows nice convergence with respect to the unit cell size.[54] In the third approach of Slater's transition state, we expand the total energy in terms of orbital occupation number around half occupation and approximate eq 1 as

$$E_b(\mathrm{N1s};\Delta\mathrm{Slater}) = \left(\frac{\partial}{\partial n_v} - \frac{\partial}{\partial n_c}\right)E(n_c,n_v)|_{n_c=n_v=1/2} = \varepsilon_F(1/2,1/2) - \varepsilon_{1s}(1/2,1/2) \quad (2)$$

In the above equation, $\varepsilon_F(1/2,1/2)$ denotes practically the Kohn−Sham orbital energy of HOMO with orbital occupations set to half 1s core electron and half electron in HOMO and $\varepsilon_{1s}(1/2,1/2)$ is the Kohn−Sham 1s core level with the same orbital occupation. This is the standard prescription of Slater's transition state. However, we found that introduction of half hole to HOMO destabilizes the self-consistent calculation. Noting that the wave function of HOMO is extended, we expect that the effect of half-hole at HOMO must be quite small and decided to neglect it. Therefore, in the present work, we adopt the following expression for the core-level binding energy in Slater's transition state:

$$E_b(\mathrm{N1s};\Delta\mathrm{Slater}) = \varepsilon_F(1/2,1) - \varepsilon_{1s}(1/2,1) \quad (3)$$

where the occupation number of HOMO is set to unity. We tested the effect of half electron in HOMO for some cases (graphite-like N in the armchair ribbon, cyanide-like N located along armchair and zigzag edges) and found that the 1s binding energy changes only by 0.1 eV.

3. RESULTS AND DISCUSSION

3.1. Relative Stability of Nitrogen Dopant Configurations along Edges. Before showing results of the spectral features of N-graphene, the relative stability of some configurations of doped N along armchair and zigzag edges is discussed in this subsection. Note that the present discussion will be made only on some limited range of configurations. This is because the way of termination of edge C will strongly affect the stability of nitrogen dopant and very extensive work is needed for more comprehensive analysis of relative stability among several different configurations of doped N. We leave such a study as our future task.

We already studied different distributions of graphite-like N along zigzag edge with various ratios between mono- and dihydrogenation[29] and found that with increasing the concentration of dihydrogenated edge-carbons, the catalytically active graphite-like N site next to the zigzag edge can be stabilized. Furthermore, the stability of pyridinium-like N dopant along zigzag edges was also investigated,[26] and our results show that it is unlikely for two N dopants to be located at neighboring sites of the edge, due to large energy difference amounting to ∼1.0 eV between close and distant two doped nitrogens. Thus for zigzag edges, a single pyridinium-like N (z_{pydm}) at site 1 (Figure 1b) is investigated in this study. Our

dx.doi.org/10.1021/jp307405r | J. Phys. Chem. A 2013, 117, 579−589

previous study also suggests that z_{pydm} and pyridine-like N (z_{pyd}) tend to be stabilized by mono- (C_H) and dihydrogenation (C_{H2}) of neighboring carbons along zigzag edges, respectively.[29] Accordingly, we consider three variants of pyridine-like N at site 2 ($C_Hz_{pyd}C_H$), 3 ($C_{H2}z_{pyd}C_H$) and 4 ($CH_2z_{pyd}C_{H2}$) as shown in Figure 1b. Here, the symbol of $C_{H2}z_{pyd}C_H$ denotes that one of two neighboring edge-carbons of z_{pyd} is dihydrogenated whereas another one is monohydrogenated.

For armchair edges, as far as we noticed, detailed theoretical study on possible configurations of N dopant has not been reported so far. Therefore, we first examine them using a model containing two pyridine-like (a_{pyd}) or two pyridinium-like N (a_{pydm}) along armchair edges as shown in Figure 1a. We deal with three configurations of a pair of N atoms at sites (0, 1), (0, 2), and (0, 3), which are denoted, respectively, as near, middle, and far configurations below. For example, a_{pyd}^{near} means that two pyridine-like N atoms are substituted for C atoms at site 0 and 1. The reason of this analysis is that according to our preliminary simulation study on the ORR process, the a_{pyd}^{middle} configuration seems to catalyze two successive two-electron ORRs to fully reduce an oxygen molecule to two water molecules. Therefore, we want to obtain information about the stability of the configuration and at the same time any possibility of identification of the configuration. By taking the total energy of a_{pydm}^{far} or a_{pyd}^{far} as the reference of the corresponding type of N configuration, the relative energies for different configurations of two N dopants at armchair edges are shown in Table 1. For both types of N dopant, the relative energy increases with decreasing the distance between two nitrogens. Note that the energy for a_{pyd}^{middle} (a_{pydm}^{middle}) estimated as 0.15 (0.31) eV is much smaller than the corresponding estimate for zigzag edge of ~1.0 eV as already mentioned. This implies that contrary to the situation of zigzag edge, some amount of particular N configurations of a_{pydm}^{middle} and a_{pyd}^{middle} may exist along armchair edge. Thus, the X-ray spectra of pyridinium-like and pyridine-like N along armchair edge in far and middle configurations are also investigated in the next subsection.

For amine-like N, four models were treated as shown in Figure 2. Along both armchair and zigzag edges, parallel configurations ((a) and (c)) are more stable than perpendicular ones ((b) and (d)) with the energy difference being 0.24 eV/NH_2 for armchair edge and 0.16 eV/NH_2 for zigzag edge. As the perpendicular configuration can be easily converted to a parallel one without any atomic diffusion, we conclude that the amine configuration will take the parallel configuration. Therefore, the spectral features for amine-like N will be presented only for the parallel configurations. Panels a and b of Figure 4 show the optimized structures for parallel configuration. Analogously to NH_3, NH_2C moiety is not planar and causes significant corrugation of graphene ribbons. The bond angle sum around N is 340° for armchair case and 343° for zigzag case.

For the pyrrole-like N, two different local environments of N are considered in the cluster calculations as shown in Figure 3. We first thought that the pyrrole-like configuration of Figure 3a may have stronger constraint for structural relaxation from the surrounding graphene structure than that of Figure 3b. However, the former is more stable than the latter by about 0.3 eV. In Figure 3, Clar sextet circles are denoted by circles and C−C double bonds by red bars. There is no dangling bond in both configurations and the number of Clar sextet circles is the same between them. Because of the energy difference, the configuration of Figure 3a may be more populated than that of Figure 3b. Nevertheless, once the configuration of Figure 3b is realized by some kinetic reasons, it may stay as a local stable configuration because of the difficulty of N diffusion. Therefore, spectral features will be discussed for both configurations.

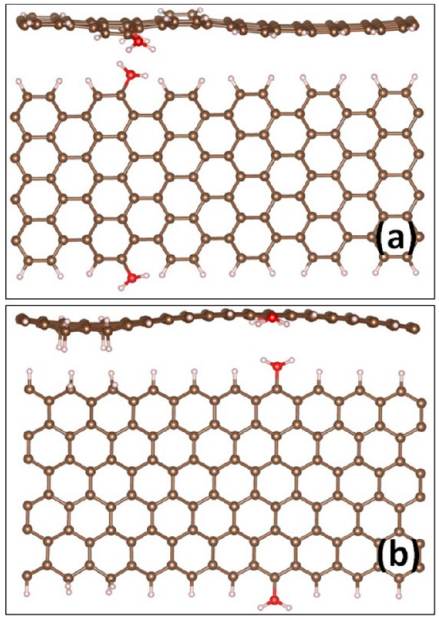

Figure 4. Optimized structures of parallel configuration of amine-like N: (a) armchair edge; (b) zigzag edge. Note that NH_2C is not planar and significant corrugation is induced in the graphene ribbon particularly for the zigzag edge case.

We investigated below the X-ray spectra for six categories of N configurations with each category containing some possible variations as listed in the left end column of Table 2. They are (1) three types of graphite-like N, located inside a perfect graphene and at the centers of armchair ribbon and zigzag ribbon; (2) three types of pyridinium-like N, along armchair edge in far (a_{pydm}^{far}) and middle (a_{pydm}^{middle}) configurations and along zigzag edge (z_{pydm}); (3) one pyrrole-like N (a_{pyrr}) located at armchair edge of a ribbon and two additional ones as shown in Figure 3a,b; (4) two types of amine-like N, along armchair (a_{am}) and zigzag (z_{am}) edges as shown in Figure 4a,b; (5) two types of cyanide-like N, along armchair (a_{cn}) and zigzag (z_{cn}) edges; (6) two types of pyridine-like N along armchair edge (a_{pyd}^{far} and a_{pyd}^{middle}) and three types of pyridine-like N along zigzag edge with different H terminations at the neighboring edge C sites as denoted as $C_{H2}z_{pyd}C_{H2}$, $C_{H2}z_{pyd}C_H$, and $C_Hz_{pyd}C_H$, where C_{H2} and C_H denote di- and monohydrogenation, respectively.

3.2. Nitrogen 1s Binding Energies. Because synthesized graphene samples contain much larger interior area than that of edges, the X-ray spectrum of N dopant in the bulk of graphene, i.e., graphite-like N, exhibiting well resolved spectral features, is the reference for characterizing the N configurations. Thus, the spectral features of graphite-like N have first been investigated by using the supercell (Figure 5) containing 336 atoms and armchair (Figure 1a) and zigzag (Figure 1b) ribbons where nitrogen is doped at each central position. The calculated N 1s binding energies (BEs), which are estimated with respect to the Fermi level (E_F) by the initial Kohn−Sham (KS) 1s energy level, the total energy difference (ΔSCF) and Slater's transition state method (Slater), are listed in Table 2 along with some

Table 2. Simulated Binding Energies (BEs) of N 1s Core Level with Respect to the Fermi Level by the Initial Kohn−Sham Energy Level (KS), ΔSCF and Slater's Transition State (Slater)[a]

N configuration	KS (eV)	ΔSCF (eV)	Slater (eV)	exp (eV)
		Graphite-like		
infinite	379.9	400.2	402.0	
armchair	380.1 (0.2)	400.2 (0.0)	402.2 (0.2)	
zigzag	380.1 (0.2)	400.2 (0.0)	402.0 (0.0)	
				402.7 (0.0)[b]
				401.7 (0.0)[c]
				401.3 (0.0)[d]
		Pyridinium-like		
a_{pydm}^{far}	379.7 (−0.2)	400.0 (−0.2)	401.8 (−0.2)	
a_{pydm}^{middle}	379.5 (−0.4)	399.9 (−0.3)	401.8 (−0.2)	
z_{pydm}	379.4 (−0.5)	399.2 (−1.0)	401.4 (−0.6)	
		Pyrrole-like		
a_{pyrr}	378.7 (−1.2)	399.5 (−0.7)	401.0 (−1.0)	
$c_{pyrr}^{3(a)}$	378.6 (−1.3)	398.8 (−1.4)[e]	400.6 (−1.4)	
$c_{pyrr}^{3(b)}$	378.7 (−1.2)	399.1 (−1.1)[f]	400.9 (−1.1)	
				401.2 (−1.5)[b]
				400.1 (−1.6)[c]
				400.0 (−1.3)[d]
		Amine-like		
a_{am}	377.3 (−2.6)	398.8 (−1.4)	401.0 (−1.0)	
z_{am}	377.4 (−2.5)	398.9 (−1.3)	400.1 (−1.9)	
		Cyanide-like		
a_{cn}	376.3 (−3.6)	397.0 (−3.2)	399.4 (−2.6)	
z_{cn}	376.4 (−3.5)	396.6 (−3.6)	398.6 (−3.4)	
		Pyridine-like		
a_{pyd}^{far}	376.4 (−3.5)	396.9 (−3.3)	399.1 (−2.9)	
a_{pyd}^{middle}	376.2 (−3.7)	396.8 (−3.4)	399.0 (−3.0)	
$C_{H2}z_{pyd}C_{H2}$	376.2 (−3.7)	396.5 (−3.7)	399.1 (−2.9)	
$C_{H2}z_{pyd}C_{H}$	376.3 (−3.6)	396.6 (−3.6)	398.7 (−3.3)	
$C_{H}z_{pyd}C_{H}$	376.4 (−3.5)	396.0 (−4.2)	397.9 (−4.1)	
				399.1 (−3.6)[b]
				398.2 (−3.5)[c]
				398.4 (−2.9)[d]

[a]The N 1s chemical shifts defined as BE(given configuration) − BE(graphite-like N in infinite graphene) are given in parentheses. Some experimental results are also presented. [b]Reddy et al.[16] [c]Wei et al.[32] [d]Niwa et al.[31] [e]Pyrrole-like N in Figure 3a. [f]Pyrrole-like N in Figure 3b.

experimental results. Because different experimental results show different absolute values of N 1s BEs depending on experimental conditions, for example the use of different substrates for graphene growth,[8] the N 1s chemical shift for a given configuration of doped N defined as δBE = BE(given N-configuration) − BE(graphite-like N) is more meaningful and presented in parentheses of Table 2. Note that we take the graphite-like N in an infinite graphene as the reference even for the N configurations treated with armchair and zigzag ribbons. This is based on the observation that the use of a ribbon is a fairly good approximation for the electronic structure of an atom along the edge of a semi-infinite plane even if the central atom of a ribbon is a rather poor approximation of an atom in an infinite plane.[56]

Before going into the details, we first discuss overall aspects seen in Table 2. As we expect, the chemical shifts obtained by ΔSCF and Slater's transition state are fairly close to each other. However, more attention should be paid to the fact that they semiquantitatively agree with those obtained by KS energy levels, implying that the N 1s chemical shift is dominated by the initial-state effect. This aspect was already pointed out by Casanovas et al.[44] and observed in our previous work[29] and also in our recent work.[54] Note that the final-state effect is more important than the initial state effect for the carbon chemical shifts in graphene.[28] Another aspect we find in Table 2 is that the absolute values of N 1s binding energy estimated by Slater's transition state (eq 3) agree quite well even quantitatively with experimental data, whereas ΔSCF results underestimate them by about 2.0 eV. Nevertheless, as Slater's transition state is an approximation to ΔSCF, the following quantitative analysis will be made using ΔSCF results.

We show in Figure 6 the chemical shifts obtained by ΔSCF in Table 2 together with the experimental XPS peaks, for which not only the peak positions but also a peak width of 1.5 eV are indicated. The members in each of the two doublets (a_{pydm} and a_{pyd}) correspond to "far" and "middle" configurations along the armchair edge. Using this figure, we make some comments on the identification of each N configuration and possible components in each experimental peak. For pyridinium-like N, those along the armchair edge may contribute to the peak III, which is usually assigned to graphite-like N, whereas those along zigzag edge may belong to the peak II which is usually assigned to pyrrole-like N. In the experimental analysis, possibility of pyridinium-like N has never been considered. The calculated chemical shift for pyrrole-like N (a_{pyrr}) for the armchair ribbon may be slightly too small. On this aspect, we

dx.doi.org/10.1021/jp307405r | J. Phys. Chem. A 2013, 117, 579−589

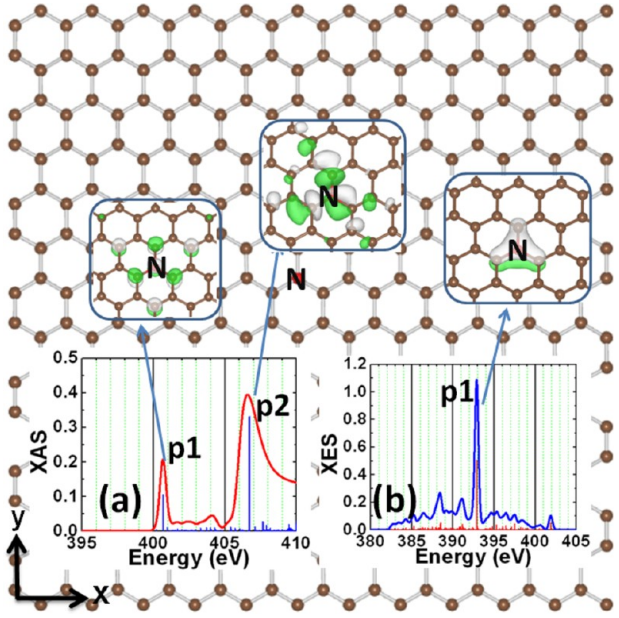

Figure 5. Supercell of infinite graphene with N dopant at interior site. The XAS and XES of graphite-like N are shown in the insets of (a) and (b), respectively. The final (initial)-state wave functions corresponding to peak p_1^{XAS} and p_2^{XAS} (p_1^{XES}) are also shown in the insets for XAS (XES).

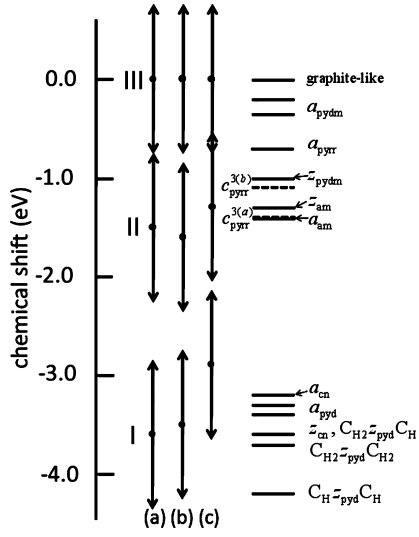

Figure 6. Horizontal bars show the ΔSCF chemical shifts of N 1s core-level binding energy for various configurations of doped N along graphene edges. The broken bars denoted as $c_{pyrr}^{3(a)}$ and $c_{pyrr}^{3(b)}$ are the chemical shift of pyrrole-like N calculated for cluster models in Figure 3. Experimental XPS peak positions together with peak width of 1.5 eV are shown for three different experiments: (a) ref 15; (b) ref 31; (c) ref 30.

speculate that the pyrrole configuration shown at the bottom of Figure 8 may have strong structural constraint by the substrate graphene. Therefore, we tried to use a cluster model for pyrrole-like N, as shown in Figure 3a,b, and obtained chemical shifts of −1.4 (Figure 3a) and −1.1 eV (Figure 3b) depending on the local environment. These values are included in Table 2 and also shown in Figure 6 as $c_{pyrr}^{3(a)}$ and $c_{pyrr}^{3(b)}$. As suggested by the experimental width of XPS peak, the chemical shift of pyrrole-like N may spread widely depending on the local environment.

On the other hand, amine-like N, whose chemical shifts are shown as a_{am} and z_{am} corresponding to Figure 4a,b, will contribute to the peak II and this assignment is consistent with the experimental analysis.[37] Up to here, all hydrogenated N including pyridinium-like N, pyrrole-like N, and amine-like N have chemical shifts within 1 eV, suggesting that identifying the specific configuration of hydrogenated nitrogen by using XPS technique is not easy.

Our result for cyanide-like N indicates that it contributes to peak I, which is generally assigned to pyridine-like N. This is different from the experimental analysis,[39] which assigned the peak II to cyanide-like N. As for pyridine-like N, the chemical shifts for a_{pyd}^{far} (3.3 eV), a_{pyd}^{middle} (3.4 eV), $C_{H2}z_{pyd}C_{H2}$ (3.7 eV), and $C_{H2}z_{pyd}C_H$ (3.6 eV) are certainly in the range of the peak I.[57,58] For $C_Hz_{pyd}C_H$, however, its chemical shift is estimated as large as 4.2 eV, suggesting that monohydrogenated zigzag edge-carbons are rare around pyridine-like N in real samples, being consistent with the result of our previous paper that the configuration is locally unstable.[29]

3.3. Graphite-like N K-Edge XAS and XES. Figure 5 shows the simulated graphite-like N K-edge XAS and XES together with final- and initial-state wave functions for XAS and XES, respectively. Two well-resolved resonance peaks are seen in the computed XAS at 400.8 (p_1^{XAS}) and 406.5 eV (p_2^{XAS}), in good agreement with the observed two prominent peaks located at 399.8−402.0 and 406−407.0 eV assigned commonly to graphite-like N.[35,41,30] By comparing the computed XAS with the density of states (DOS) of graphite-like N p orbitals shown in Figure 7a, we can find that p_1^{XAS} (p_2^{XAS}) of graphite-like N corresponds to the transition of N 1s core states to π^* (N−C

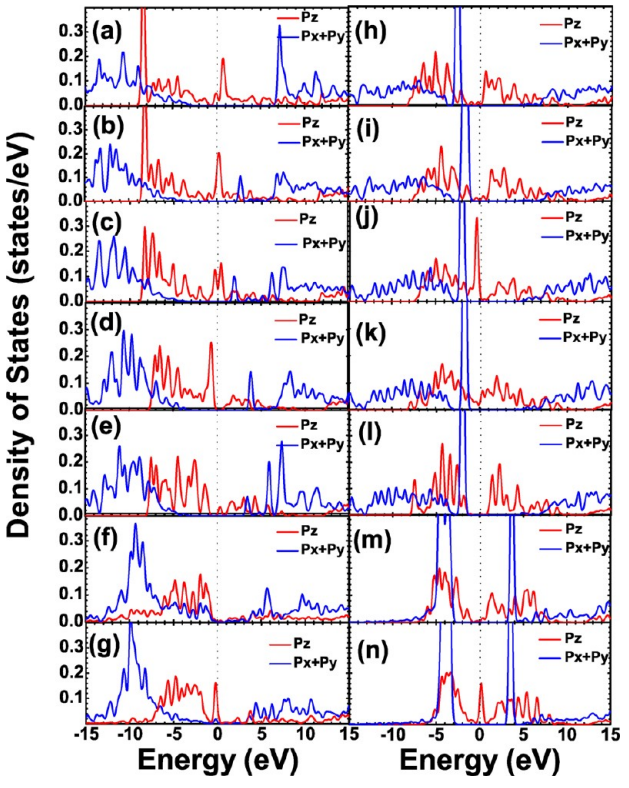

Figure 7. Density of states (DOS) of p orbitals for N dopant in infinite graphene (a) and at the graphene edges in the configurations of a_{pydm}^{far} (b), a_{pydm}^{middle} (c), z_{pydm} (d), a_{pyrr} (e), a_{am} (f), z_{am} (g), a_{pyd}^{far} (h), a_{pyd}^{middle} (i), $C_Hz_{pyd}C_H$ (j), $C_{H2}z_{pyd}C_H$ (k), $C_{H2}z_{pyd}C_{H2}$ (l), a_{cn} (m), and z_{cn} (n).

dx.doi.org/10.1021/jp307405r | J. Phys. Chem. A 2013, 117, 579−589

σ^*) located at ~1 (7) eV above E_F. These assignments are confirmed by the analysis of final-state wave functions shown in the inset of Figure 5. On the other hand, the XES of graphite-like N shows a single sharp peak at 393 eV (p_1^{XES}), which is contributed by occupied π states as shown in the inset of Figure 5. The peak position of p_1^{XES} corresponds to the bottom of the π band (about 8.5 eV deep from the Fermi level) where the π component of density of states (DOS) at N has a sharp peak as shown in Figure 7a. These spectral features agree with our previous results where graphite-like N was doped into the center site of graphene zigzag ribbon.[29] However, as shown in our previous work, the spectral features of graphite-like N will change with its location and chemical environments,[29] for example, the BE of graphite-like N at the site next to standard zigzag edge (edge-1 site for short), where all edge carbons are monohydrogenated, is about 0.6 eV larger than that of N at the interior site. It was also shown[29] that in contrast to the XAS of graphite-ike N at the interior site, one additional small peak just below p_2^{XAS} peak is observed in the XAS spectra of all graphite-like N at the zigzag edge-1 site (N^{edge-1}). Furthermore, in the presence of dihydrogenated edge-carbons, the intensity of the first XAS peak of N^{edge-1} is reduced whereas its XES main peak will be shifted down.

3.4. XAS and XES of N at Edge Sites. In this subsection, we first present the computed K-edge XAS and XES of hydrogenated N and then discuss the spectral features of non-hydrogenated one both along two edges. To understand the basic electronic structures of those configurations, DOS of p orbitals for each configuration is shown in Figure 7.

3.4.1. Hydrogenated (Pyridinium-like and Pyrrole-like) N. Figure 8 shows the computed XAS and XES of pyridinium-like and pyrrole-like N, both of which are monohydrogenated. Similarly to the graphite-like N XES, only one single sharp peak (p_1^{XES} at 393 eV) due to the N−C π bonds (see top and bottom panels of Figure 8) is observed in all monohydrogenated N K-edge XES. The situation remains the same in the cluster configurations of pyrrole-like N (Figure 3). The position of p_1^{XES} corresponds to the bottom of π band like in the case of graphite-like N. Even if there is no very sharp peak in the π component of DOS at N at the π band bottom (for example, for z_{pydm} and a_{pyrr}), the presence of a core hole will produce a peak there. Moreover, the reason why the sharp π state peak just below the Fermi level for z_{pydm} does not show up in its XES is also explained by the effect of core hole. Anyway, one cannot distinguish monohydrogenated N from graphite-like one using XES alone. On the other hand, in the monohydrogenated N K-edge XAS shown in Figure 8a−d, besides peak p_1^{XAS} and p_2^{XAS} an additional peak is observed at ~402 eV (p_3^{XAS}) between p_1^{XAS} and p_2^{XAS} though the intensity of p_1^{XAS} is quite weak for z_{pydm} and a_{pyrr}. From the analysis of final-state wave functions shown in the top and bottom panels of Figure 8, the p_3^{XAS} peak is found to be contributed by the N−H σ^*. This is confirmed by examining the DOS of a_{pydm}^{far}, a_{pydm}^{middle}, z_{pydm}, and a_{pyrr} as shown in Figure 7. Obviously, a σ^* bond originating from the hybridization between N p and H s orbitals is commonly observed at ~3.0 eV above E_F. Although graphite-like and H-terminated N have three nearest neighbors, all of them are carbons for the former N and one nearest neighbor is hydrogen for the latter. Hence, p_3^{XAS} peak contributed by N−H σ^* orbitals can be regarded as a fingerprint of hydrogenated N in N-graphene. This aspect is basically valid as seen below even for amine-like N which has two hydrogens.

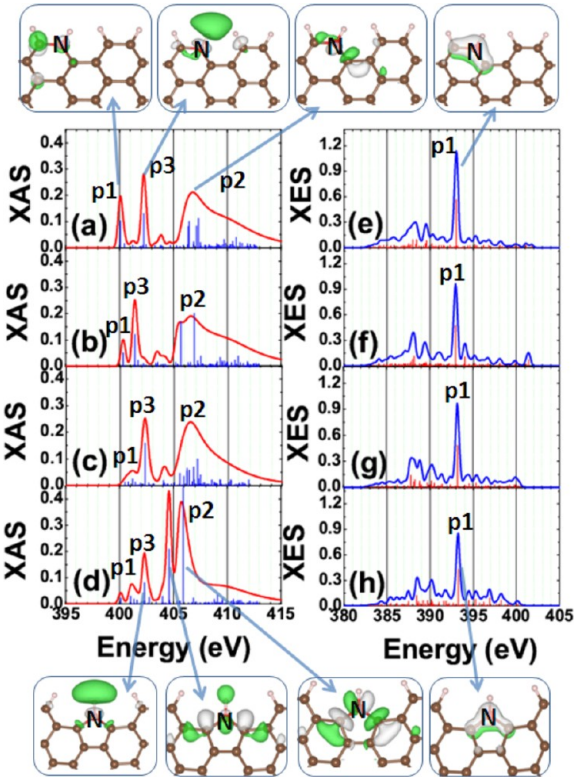

Figure 8. Calculated XAS (XES) spectra of N in the configurations of a_{pydm}^{far}, a_{pydm}^{middle}, z_{pydm}, and a_{pyrr} are shown in a (e), b (f), c (g), and d (h), respectively. The final (initial)-state wave functions corresponding to some prominent peaks of XAS (XES) are shown in top and bottom panels.

Note that p_2^{XAS} of pyrrole-like N, which is contributed by N−C σ^* bonds, is shifted down from the corresponding peak of pyridinium-like N by about 1.5 eV due to slightly elongated N−C bond and split into two peaks located at 404.5 and 406 eV, respectively. The lower component of 404.5 eV is unique to pyrrole-like N and can be used to identify it. By the analysis of final-state wave functions (see bottom panels of Figure 8) for these two peaks, the splitting is due to the interaction between N−H σ^* bond and N−C σ^* bonds. It is also important to note that the final state wave function of 404.5 eV peak extends to the second nearest neighbor C of N. Therefore, the presence of this peak may depend on the details of the atomic configuration at the surrounding sites. This is clearly supported by the XAS for the two configurations of pyrrole-like N in Figure 3. The local configuration in Figure 3a is basically the same as that of Figure 8d, and their XAS are basically the same. On the other hand, the pyrrole-like N located at the corner of graphene cluster (Figure 3b) does not show the peak at 404.5 eV, suggesting that the presence of the peak depends on the local configuration around pyrrole-like N. However, as the configuration of Figure 3a is more stable than that of Figure 3b, the peak at 404.5 eV will still be a characteristic feature of pyrrole-like N.

As for amine-like N with two hydrogen atoms, we note that there is virtually no difference in the XES between armchair and zigzag edges (Figure 9b,d) and that in addition to p_1^{XES} observed for monohydorogenated N cases, their XES shows another large peak (p_2^{XES} at 388−399 eV) contributed by in-plane π orbital with bonding N−H character as depicted in the top and bottom panels of Figure 9, indicating that amine-like N can be

dx.doi.org/10.1021/jp307405r | J. Phys. Chem. A 2013, 117, 579−589

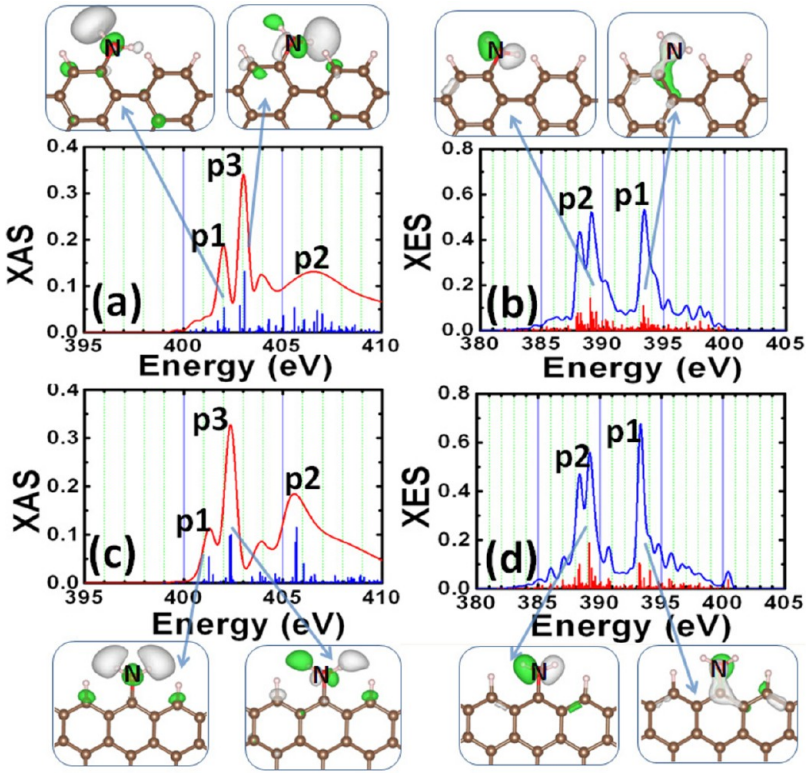

Figure 9. Calculated XAS (a, c) and XES (b, d) spectra of N in the configurations of a_{am} and z_{am}, respectively. The final (initial)-state wave functions corresponding to some typical peaks of XAS (XES) are shown in the top and bottom panels.

distinguished from monohydrogenated and graphite-like one through XES analysis.

To understand the XAS of amine-like N, it is important to note that the NH_2C moiety is not planar and that the sp^3 bonding character modifies the electronic structure near the Fermi level. From DOS shown in Figure 7f,g, it is clear that the DOS of π^* is strongly suppressed just above the Fermi level. This is the reason of the absence of a peak of π^* character and the smooth rising up of XAS near the lower binding energy edges. The sp^3 bonding character also causes mixture of σ and π symmetries. Anyway, the two peaks for both edges are mostly characterized as σ^* between N and H (see the top and bottom panels of Figure 9).

3.4.2. Nonhydrogenated (Pyridine-like and Cyanide-like) N. The spectra of pyridine-like N are shown in Figure 10. The XAS spectra of pyridine-like N have some characteristic features compared with those of graphite-like, pyridinium-like and pyrrole-like N. The peak positions of p_1^{XAS} and p_2^{XAS} are shifted down by 2−2.5 eV. This is correlated with the shallow 1s core level as shown in Table 2. The p_1^{XAS} peak is sharp and strong for a_{pyd}^{far}, a_{pyd}^{middle}, and z_{pyd} with the $C_{H2}z_{pyd}C_{H2}$ configuration, whereas it is very broad for z_{pyd} of $C_Hz_{pyd}C_H$ and $C_{H2}z_{pyd}C_H$. In contrast to XAS, the prominent peak (p_1^{XES}) of pyridine-like N K-edge XES (Figure 10f−j) at 395.0−395.5 eV is 2.0−2.5 eV higher than that of pyridinium-like and graphite-like N. This inverse correlation with the 1s core level chemical shift is due to the difference in the energy level of the initial state. Though p_1^{XES} of pyridinium-like and graphite-like N corresponds to the bottom of the π band being 8.5 eV deep from the Fermi level, p_1^{XES} of pyridine-like N comes form the sharp peak of σ state only within the rage of 0.2 eV below the Fermi level as suggested by the DOS for pyridine-like N depicted in Figure 7h−l together with the initial-state wave function (see right top panel of

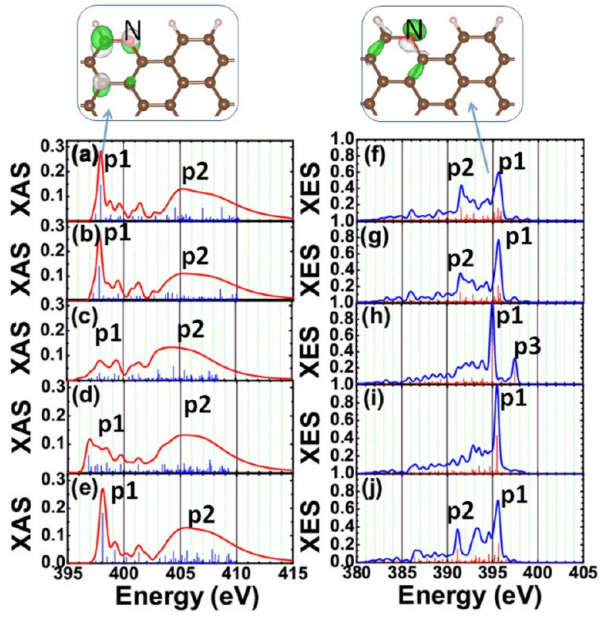

Figure 10. Calculated XAS (a−e) and XES (f−j) spectra of N in the configurations of a_{pyd}^{far}, a_{pyd}^{middle}, $C_Hz_{pyd}C_H$, $C_{H2}z_{pyd}C_H$, and $C_{H2}z_{pyd}C_{H2}$, respectively. The final (initial)-state wave functions corresponding to peak p_1^{XAS} (p_1^{XES}) of XAS (XES) are shown in the top panels.

Figure 10). This sharp σ peak corresponds to the lone paired two N σ electrons. On the other hand, another less prominent peak p_2^{XES} in Figure 10 comes from the bottom of π band. On the basis of the symmetry consideration of XES peaks, we conclude that pyridine-like N can be identified by analyzing the features of not only XPS but also XES. Note that the spectral

dx.doi.org/10.1021/jp307405r | J. Phys. Chem. A 2013, 117, 579−589

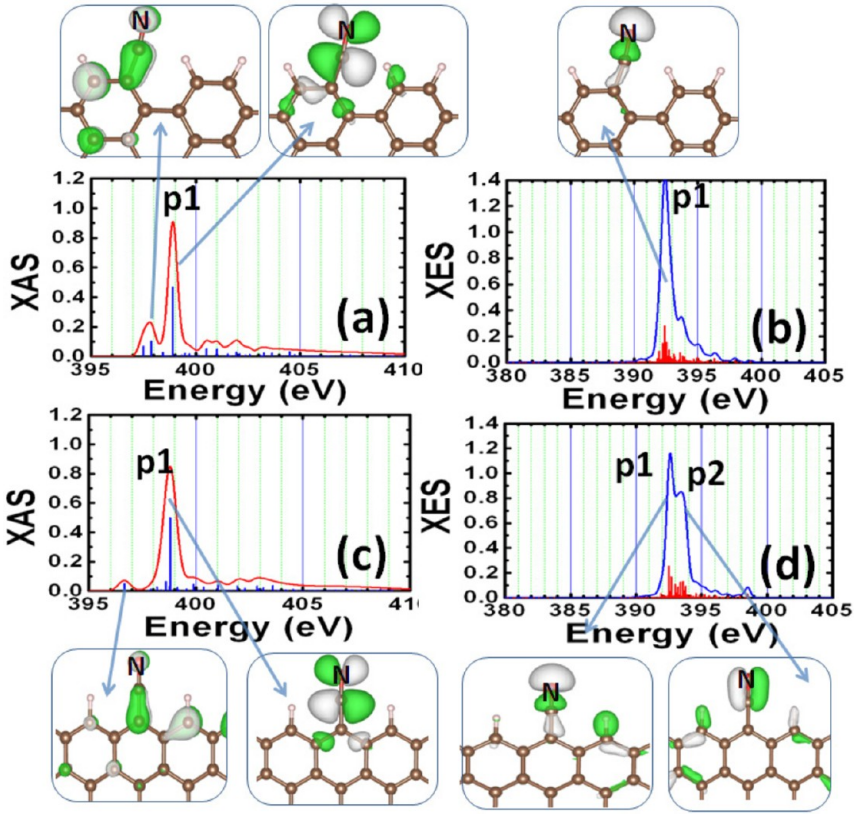

Figure 11. Calculated XAS (a, c) and XES (b, d) spectra of N in the configurations of a_{cn} and z_{cn}, respectively. The final (initial)-state wave functions corresponding to some typical peaks of XAS (XES) are shown in top and bottom panels. .

features (shown in Figure 10e,j) and DOS (shown in Figure 7l) of $C_{H2}z_{pyd}C_{H2}$ are quite similar to those of pyridine-like N along armchair edge. However, as we pointed out,[57] the population of $C_{H2}z_{pyd}C_{H2}$ will be quite small and then pyridine-like N located at the armchair edge can be identified easily by its characteristic feature in XES. We also point out that the pyridine-like N with the $C_Hz_{pyd}C_H$ configuration, if it may exist, can be easily identified by XES because of the presence of an additional peak p_3^{XES} at 397.5 eV as seen in Figure 10h. There are no other N configurations treated in our work which show a peak near this peak position. From electronic structure analysis (Figure 7j), this peak is contributed by π orbital.

The XAS and XES for cyanide-like N are shown in Figure 11. Both along armchair and zigzag edges, XAS of cyanide-like N has a sharp main peak and a small subpeak located in the lower binding energy side. The final state wave functions shown in the top and bottom panels of Figure 11 indicate that the small lower energy peak originates from the transition to rather delocalized π^* states and that the main peak is due to the in-plane π^* state localized at the terminal C−N for both edges. As it will be difficult to identify the small peaks experimentally in both cases, the XAS of cyanide-like N will be characterized by the main peaks p_1^{XAS}. As for XES, a sharp peak p_1^{XES} is accompanied by a weak shoulder in the higher energy side for armchair edge, whereas the shoulder p_2^{XES} is larger for the zigzag edge. The p_1^{XES} peak originates from C−N−C σ state whereas the shoulder p_2^{XES} mostly comes from in-plane bonding π state for the terminal C−N.

3.4.3. Comparison with Experiment. As we pointed out, cyanide-like and pyridine-like N will contribute to an overlapping peak in N 1s XPS. As shown in Figure 11a,c, we observe a sharp XAS peak (p_1^{XAS}) of cyanide-like N at about 399 eV, which is 1.0 eV higher than that of pyridine-like N, whereas the prominent XAS peak of amine-like N is located at 402.8 eV. The results thus indicate that cyanide-like and pyridine-like N can be distinguished by using XAS, which was actually done by Niwa et al.[30] Moreover, we note that the final state of the p_1^{XAS} peak of cyanide-like N is a π state confined within the graphene plane, which has different photon-polarization dependence from the other π transition. By using the Photon Factory (KEK), Niwa et al.[30] observed four peaks at the N K-edge XAS of CoPc based N-graphene (1% N concentration) and assigned peak A1 (399.1 eV), A2 (400.1 eV), and A3 (401.5 eV) to pyridine-like, cyanide-like, and graphite-like N, respectively, whereas A4 at ∼407 eV is attributed to the transition from N 1s core states to N−C σ^* bonds. Recently, by using SPring-8, Saito et al. performed more precise XAS measurements of N-graphene (8% N concentration) synthesized from FePc and observed the A1, A2, A3, and A4 peaks at 398.0, 399.0, 401.0, and 407.0 eV,[59] in good agreement with our calculated results where the first peak of pyridine-like N (A1: see Figure 10a), the main peak of cyanide-like N (A2: see Figure 11a,c), the first (A3: see Figure 5a) and second (A4: see Figure 5a) peaks of graphite-like N are located at 398.0, 399.0, 400.8, and 406.5 eV, respectively.

4. SUMMARY

Figure 6 is a summary of calculated chemical shifts of N 1s binding energy together with experimental XPS peaks. Peak I, which is usually assigned to pyridine-like N, will have contributions also from cyanide-like N. Peak II assigned to pyrrole-like N may contain contributions from both amine-like

dx.doi.org/10.1021/jp307405r | J. Phys. Chem. A 2013, 117, 579−589

N along both edges (armchair and zigzag) and pyridinium-like N located at zigzag edge, and peak III assigned to graphite-like N may contain contributions from pyridinium-like N along armchair edge.

A summary of prominent peaks in XAS spectra is given in Figure 12. Experimental peak positions are also shown in this figure. The four components from the lower excitation energy are assigned to pyridine-like N, cyanide-like N, graphite-like N, and σ^*. In comparison to XPS spectra, cyanide-like N is explicitly taken into account and pyrrole-like N is not explicitly considered. We explain the reason why it is so. The basic difference between XPS and XAS comes from the final state. For XPS, the 1s binding energy is measured with reference to the Fermi level which has nothing to do with the final state, whereas for XAS, peaks are contributed by only those unoccupied states which have significant amplitude of the wave function in the region of the particular 1s state and are connected to the 1s state by the dipole selection rule. For cyanide-like N, Figure 7m,n show that a sharp DOS for the in-plane p orbitals is located at 3.5 eV above the Fermi level, whereas for pyridine-like N the π^* DOS is centered at around 2 eV above the Fermi level (Figure 7h–l). Therefore, the first prominent peak p_1^{XAS} of cyanide-like N is about 1 eV higher than that of pyridine-like N making the "cyanide" peak distinguishable from "pyridine" peak. Furthermore because p_1^{XAS} of cyanide-like N has in-plane π^* character, the photon polarization dependence will make the distinction clearer. Similarly, lower energy π^* peak(s) of pyrrole-like N have very weak intensity (Figure 8d and Figure 3a) and the lowest prominent peak p_3^{XAS} of the N–H σ origin is located at about 402 eV. Therefore, this peak may be in the tail of the "graphite" peak, which actually has a fairly broad higher energy tail,[59] and therefore may not separately be assigned. Only photon polarization dependence will help identify it. This ends the explanation why three low energy peaks are assigned differently between XPS and XAS. Some additional comments on XAS are as follows. The N–H σ peak around 402–403 eV is common to all hydrogenated N configurations. The sharp σ peak at 404.5 eV is unique to the pyrrole-like N shown in Figure 8d and Figure 3a. Although this peak is not always present for pyrrole-like N as suggested by the cluster calculation in Figure 3, we can expect that majority of pyrrole-like N will show it. Nevertheless, the results summarized in Figure 12 suggest that N configurations with N–H σ bond (pyridinium-like and amine-like) cannot be clearly identified by XAS spectra.

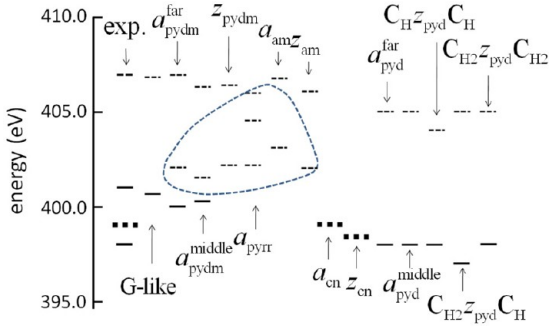

Figure 12. Summary of prominent peak positions in the calculated XAS spectra for various N configurations together with the experimental data.[59] "G-like" denotes graphite-like. Solid bars denote transition from N 1s to π^* state and dotted bars that to σ^* state. Those σ^* transitions in the enclosed region are quite sharp, whereas other σ^* transitions are broad. The thicker dotted bars for a_{cn} and z_{cn} indicate that the final state is a π^* state confined within the graphene plane.

Peak positions and peak characters for XES spectra are summarized in Figure 13. It is clear from this figure, pyridine-like N and amine-like N are easily identified by XES spectra. In addition to this, if the sample has unique direction of the graphene plane, the photon polarization dependence can identify the cyanide-like N.

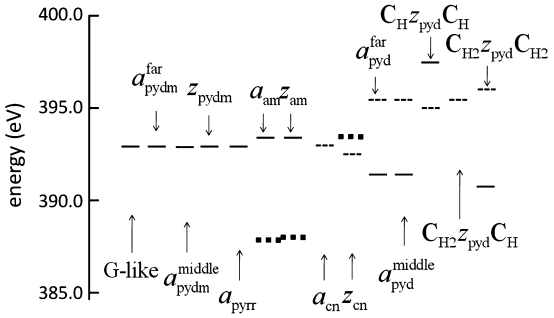

Figure 13. Summary of prominent peak positions in the calculated XES spectra for various N configurations. "G-like" denotes graphite-like. Solid bars denote transition from π state and dotted bars that from σ state. The thicker dotted bars for a_{am}, z_{am}, and z_{cn} indicate that the initial state is a π^* state confined within the graphene plane.

As far as we know, any possibility of pyridinium-like N has never been considered in the experimental work of XPS, XAS, and XES, although such configuration will exist in real samples, as suggested by theoretical studies.[29,55] The present analysis on XPS, XAS, and XES has clarified the reason of difficulty in identifying the pyridinium-like N. Meanwhile, the present study suggests that the combined use of XPS, XAS, and XES together with theoretical analyses will be quite useful to identify most of the N configurations in graphene-based materials.

AUTHOR INFORMATION

Corresponding Author

*E-mail: xianlongwang3@gmail.com.

Present Address

⊥Geodynamics Research Center, Ehime University, 2-5 Bunkyo-cho, Matsuyama, Ehime 790- 8577, Japan.

Notes

The authors declare no competing financial interest.

ACKNOWLEDGMENTS

This work was supported by Project 10000832-0 of the New Energy Industrial Technology Development Organization (NEDO). The present computations were performed using the supercomputing facilities in JAIST and JAEA.

REFERENCES

(1) Novoselov, K. S.; Geim, A. K.; Morozov, S. V.; Jiang, D.; Zhang, Y.; Dubonos, S. V.; Grigorieva, I. V.; Firsov, A. A. *Science* **2004**, *306*, 666.

(2) Zhou, S. Y.; Gweon, G. -H.; Fedorov, A. V.; First, P. N.; de Heer, W. A.; Lee, D. -H.; Guinea, F.; Castro Neto, A. H.; Lanzara, A. , *Nature Mater.* **2007**, *6*, 770.

(3) Shemella, P.; Nayak, S. K. *Appl. Phys. Lett.* **2009**, *94*, 032101.

(4) Cuong, N. T.; Otani, M.; Okada, S. *Phys. Rev. Lett.* **2011**, *106*, 106801.

(5) Wang, X.; Li, X.; Zhang, L.; Yoon, Y.; Weber, P. K.; Wang, H.; Guo, J.; Dai, H. *Science* **2009**, *324*, 768.
(6) Imamura, G.; Saiki, K. *J. Phys. Chem. C* **2011**, *115*, 10000.
(7) Zhao, W.; Höfert, O.; Gotterbarm, K.; Zhu, J. F.; Papp, C.; Steinrück, H. -P. *J. Phys. Chem. C* **2012**, *116*, 5062.
(8) Koch, R. J.; Weser, M.; Zhao, W.; Viñes, F.; Gotterbarm, K.; Kozlov, S. M.; Höfert, O.; Ostler, M.; Papp, C.; Gebhardt, J. *Phys. Rev. B* **2012**, *86*, 075401.
(9) Lin, Y. -C.; Lin, C. -Y.; Chiu, P. -W. *Appl. Phys. Lett.* **2010**, *96*, 133110.
(10) Panchakarla, L. S.; Subrahmanyam, K. S.; Saha, S. K.; Govindaraj, A.; krishnamurthy, H. R.; Waghmare, U. V.; Rao, C. N. R. *Adv. Mater.* **2009**, *21*, 4726.
(11) Shao, Y.; Zhang, S.; Engelhard, M. H.; Li, G.; Shao, G.; Wang, Y.; Liu, J.; Aksay, I. A.; Lin, Y. *J. Mater. Chem.* **2010**, *20*, 7491.
(12) Wang, X.; Zeng, Z.; Ahn, H.; Wang, G. *Appl. Phys. Lett.* **2009**, *95*, 183103.
(13) Jafri, R. I.; Rajalakshmi, N.; Ramaprabhu, S. *J. Mater. Chem.* **2010**, *20*, 7114.
(14) Zhang, C.; Fu, L.; Liu, N.; Liu, M.; Wang, Y.; Liu, Z. *Adv. Mater.* **2011**, *23*, 1020.
(15) Schedin, F.; Geim, A. K.; Morozov, S. V.; Hill, E. W.; Blake, P.; Katsnelson, M. I.; Novoselov, K. S. *Nat. Mater.* **2007**, *6*, 652.
(16) Reddy, A. L. M.; Srivastava, A.; Gowda, S. R.; Gullapalli, H.; Dubey, M.; Ajayan, P. M. *ACS Nano* **2010**, *4*, 6337.
(17) Ozaki, J.; Tanifuji, S.; Kimura, N.; Oya, A. *Carbon* **2006**, *44*, 1324.
(18) Ozaki, J.; Anahata, T.; Kimura, N.; Oya, A. *Carbon* **2006**, *44*, 3358.
(19) Ozaki, J.; Kimura, N.; Anahata, T.; Oya, A. *Carbon* **2007**, *45*, 1847.
(20) Bashyam, R.; Zelenay, P. *Nature* **2006**, *443*, 63.
(21) Gong, K.; Du, F.; Xia, Z.; Durstock, M.; Dai, L. *Science* **2009**, *323*, 760.
(22) Lefèvre, M.; Proietti, E.; Jaouen, F.; Dodelete, J. *Science* **2009**, *324*, 71.
(23) Nabae, Y.; Moriya, S.; Matsubayashi, K.; Lyth, S. M.; Malon, M.; Wu, L.; Islam, N. M.; Koshigoe, Y.; Kuroki, S.; Kakimoto, M. *Carbon* **2010**, *48*, 2613.
(24) Qu, L.; Liu, Y.; Baek, J. -B.; Dai, L. *ACS Nano* **2010**, *4*, 1321.
(25) Ikeda, T.; Boero, M.; Huang, S. -F.; Terakura, K.; Oshima, M.; Ozaki, J. *J. Phys. Chem. C* **2008**, *112*, 14706.
(26) Huang, S. -F.; Terakura, K.; Ozaki, T.; Ikeda, T.; Boero, M.; Oshima, M.; Ozaki, J.; Miyata, S. *Phys. Rev. B* **2009**, *80*, 235410.
(27) Ikeda, T.; Boero, M.; Huang, S. -F.; Terakura, K.; Oshima, M.; Ozaki, J.; Miyata, S. *J. Phys. Chem. C* **2010**, *114*, 8933.
(28) Hou, Z.; Wang, X.; Ikeda, T.; Huang, S. -F.; Terakura, K.; Boero, M.; Oshima, M.; Kakimoto, M.; Miyata, S. *J. Phys. Chem. C* **2011**, *115*, 5392.
(29) Wang, X.; Hou, Z.; Ikeda, T.; Huang, S. -F.; Terakura, K.; Boero, M.; Oshima, M.; Kakimoto, A.; Miyata, S. *Phys. Rev. B* **2011**, *84*, 245434.
(30) Niwa, H.; Horiba, K.; Harada, Y.; Oshima, M.; Ikeda, T.; Terakura, K.; Ozaki, J.; Miyata, S. *J. Power Sources* **2009**, *187*, 93.
(31) Niwa, H.; Kobayashi, M.; Horiba, K.; Harada, Y.; Oshima, M.; Terakura, K.; Ikeda, T.; Koshigoe, Y.; Ozaki, J.; Miyata, S. *J. Power Sources* **2011**, *196*, 1006.
(32) Wei, D.; Liu, Y.; Wang, Y.; Zhang, H.; Huang, L.; Yu, G. *Nano Lett.* **2009**, *9*, 1752.
(33) Nieto-Márquez, A.; Espartero, I.; Lazo, J. C.; Romero, A.; Valverde, J. L. *Chem. Eng. J.* **2009**, *153*, 211.
(34) Neidhardt, J.; Hultman, L.; Czigány, Zs. *Carbon* **2004**, *42*, 2729.
(35) Zhang, L. -S.; Liang, X. -Q.; Song, W. -G.; Wu, Z. -Y. *Phys. Chem. Chem. Phys.* **2010**, *12*, 12055.
(36) Li, X.; Wang, H.; Robinson, J. T.; Sanchez, H.; Diankov, G.; Dai, H. *J. Am. Chem. Soc.* **2009**, *131*, 15939.
(37) Arrigo, R.; Hävecher, M.; Wrabetz, S.; Blume, R.; Lerch, M.; McGregor, J.; Parrot, E. P. J.; Zeitler, J. A.; Gladden, L. F.; Knop-Gericke, A. *J. Am. Chem. Soc.* **2010**, *132*, 9616.
(38) La, Y. -H.; Jung, Y. J.; Kang, T. -H.; Ihm, K.; Kim, K. -J.; Kim, B.; Park, J. W. *Langmuir* **2003**, *19*, 9984.
(39) Ray, S. C.; Pao, C. W.; Chiou, J. W.; Tsai, H. M.; Jan, J. C.; Pong, W. F.; McCann, R.; Roy, S. S.; Papakonstantinou, P.; McLaughlin, J. A. *J. Appl. Phys.* **2005**, *98*, 033708.
(40) Pels, J. R.; Kapteijn, F.; Moulijn, J. A.; Zhu, Q.; Thomas, K. M. *Carbon* **1995**, *33*, 1641.
(41) Zhong, J.; Deng, J. -J.; Mao, B. -H.; Xie, T.; Sun, X. -H.; Mou, Z. -G.; Hong, C. -H.; Yang, P.; Wang, S. -D. *Carbon* **2012**, *50*, 335.
(42) Li, Y.; Zhao, Y.; Cheng, H.; Hu, Y.; Shi, G.; Dai, L.; Qu, L. *J. Am. Chem. Soc.* **2012**, *134*, 15.
(43) Usachov, D.; Vilkov, O.; Grüneis, A.; Haberer, D.; Fedorov, A.; Adamchuk, V. K.; Preobrajenski, A. B.; Dudin, P.; Barinov, A.; Oehzelt, M. *Nano Lett.* **2011**, *11*, 5401.
(44) Casanovas, J.; Ricart, J. M.; Rubio, J.; Illas, F.; Jiménez-Mateos, J. M. *J. Am. Chem. Soc.* **1996**, *118*, 8071.
(45) Son, Y. -W.; Cohen, M. L.; Louie, S. G. *Phys. Rev. Lett.* **2006**, *97*, 216803.
(46) Fujita, M.; Wakabayashi, K.; Nakada, K.; Kusakabe, K. *J. Phys. Soc. Jpn.* **1996**, *65*, 1920.
(47) Kan, E.; Li, Z.; Yang, J.; Hou, J. G. *J. Am. Chem. Soc.* **2008**, *130*, 4224.
(48) Zheng, X. H.; Wang, X. L.; Abtew, T. A.; Zeng, Z. *J. Phys. Chem. C* **2010**, *114*, 4190.
(49) Lippert, G.; Hutter, J.; Parrinello, M. *Theor. Chem. Acc.* **1999**, *103*, 124.
(50) The CP2K developers group, http://cp2k.berlios.de.
(51) Baroni, S.; Dorso, A. D.; S. de Gironcoli, and Giannozzi, P.; , www.qutantum-espresso.org.
(52) Perdew, J. P.; Burke, K.; Ernzerhof, M. *Phys. Rev. Lett.* **1996**, *77*, 3865.
(53) Iannuzzi, M.; Hutter, J. *J. Phys. Chem. Chem. Phys.* **2007**, *9*, 1599.
(54) Hou, Z.; Wang, X.; Ikeda, T.; Terakura, K.; Oshima, M.; and Kakimoto, M.; , to be submitted.
(55) Wassmann, T.; Seitsonen, A. P.; Saitta, A. M.; Lazzeri, M.; Mauri, F. *Phys. Rev. Lett.* **2008**, *101*, 096402.
(56) Terakura, K.; Terakura, I. *J. Phys. Soc. Jpn.* **1975**, *39*, 356.
(57) It is recently pointed out[58] that high population of dihydrogenation along zigzag edge is unlikely because the high chemical shift of hydrogen needed to realize it will convert graphene to graphane. However, as $C_{H2}z_{pyd}C_{H2}$ is locally stable, such a configuration may be realized locally.
(58) Zhang, X.; Yazyev, O. V.; Feng, J.; Xie, L.; Tao, C.; Chen, Y.-C.; Jiao, L.; Pedramrazi, Z.; Zettl, A.; Louie, S. G.; arXiv: *1205*.3516.
(59) Saito, M.; et al., the 217th Meeting of Electro Chemical Society, Abstract #502 (2010).